Differential Detection of $\pi/4$-Shifted-DQPSK for Digital Cellular Radio

Sandeep Chennakeshu, *Member, IEEE*, and Gary J. Saulnier, *Member, IEEE*

Abstract— **This paper discusses the detection of $\pi/4$-shifted-DQPSK modulation using a tangent type differential detector with an integrated symbol timing and carrier frequency offset correction algorithm. $\pi/4$-shifted-DQPSK modulation has been proposed for use in a high capacity, TDMA-based digital cellular system which is being developed in the U.S.; differential detection could potentially allow the production of low-complexity mobile units. Consequently, this paper presents results obtained using the proposed IS-54 TDMA frame structure for base to mobile transmissions. Theoretical and simulation bit-error-rate (BER) results are presented for static and Rayleigh fading channels. BER results are provided as a function of E_b/N_0 and C/I, where the interferer is a second $\pi/4$-shifted-DQPSK signal. Additional results are provided which show the BER sensitivity to Doppler frequency shifts, time delay spread, and carrier frequency offsets.**

I. Introduction

THE proposed U.S. digital cellular system will use a TDMA channel access method and a digital modulation scheme, initially providing a three-fold increase in capacity over the current analog FM cellular system. Essentially, the proposed system uses the existing 30-kHz channel structure and replaces the analog FM modulation with a digital modulation having a gross bit rate of 48.6 kbps. Each channel will be shared in a TDMA fashion, initially by three users and, sometime later, by six users. In order to achieve a bit rate of 48.6 kbps in a 30-kHz channel, a modulation with a spectral efficiency of 1.62 bits/Hz is required. In addition, it is necessary to employ some type of spectral shaping on the digital modulation to limit the adjacent channel interference (ACI).

While these requirements can be met by conventional filtered four phase modulation schemes such as QPSK and OQPSK, symmetric differential phase exchange keying [2], also known as $\pi/4$-shifted-QPSK, has some advantages for the mobile channel. The $\pi/4$-shifted-QPSK signal constellation can be viewed as the superposition of two QPSK signal constellations offset by 45 degrees relative to each other, resulting in eight phases. Symbol phases are alternately selected from one of the QPSK constellations and then the other and, as a result, successive symbols have a relative phase difference that is one of four angles, $\pm\pi/4$ and $\pm 3\pi/4$. Fig. 1 illustrates the $\pi/4$-shifted-QPSK signal constellation.

Manuscript received April 10, 1992; revised June 23, 1992.

S. Chennakeshu is with General Electric Co., Corporate Research and Development, Schenectady, NY 12301.

G. J. Saulnier is with the Electrical, Computer and Sytems Engineering Department at Rensselaer Polytechnic Institute, Troy, NY 12180-3590.

IEEE Log Number 9205014.

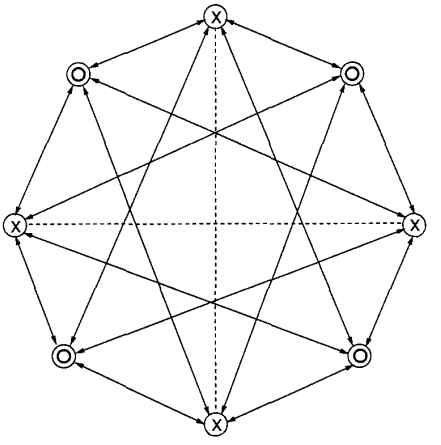

Fig. 1. $\pi/4$-shifted-QPSK signal constellation.

A number of advantages of $\pi/4$-shifted-QPSK are cited in [3] and are summarized here. A feature of this modulation is that it can be detected using a coherent detector, a differential detector, or a discriminator followed by a integrate-and-dump filter. The suitability of both differential detection and discriminator detection provides an advantage since both can be performed by low-complexity receiver structures. On the other hand, coherent detection requires a more complex receiver than either differential or discriminator detection due to the carrier recovery process. Further, in fast fading, coherent detection results in a higher irreducible BER than either differential detection or discriminator detection [3], [4]. From this view point, OQPSK, which requires coherent detection, is inferior to $\pi/4$-shifted-QPSK. Using discriminator detection for $\pi/4$-shifted-QPSK makes it easy to produce a dual-mode (digital–analog) receiver, since the discriminator can be used to detect analog FM as well as the digital $\pi/4$-shifted-QPSK modulation. Another advantage of $\pi/4$-shifted-QPSK is that unlike QPSK, the transitions in the signal constellation do not pass through the origin. As a result, the envelope of $\pi/4$-shifted-QPSK exhibits less variation than that of QPSK and, therefore, has better output spectral characteristics. However, with a reasonably linear amplifier operated with a small amount of back-off, the advantage over QPSK is negligible [11].

The proposed U.S. digital cellular system will use $\pi/4$-shifted-DQPSK [12] which is filtered at the transmitter by a square root raised cosine filter with an excess bandwidth of

0018–9545/93$03.00 © 1993 IEEE

35% (or roll-off of 0.35). A corresponding square root raised cosine filter is to be used at the receiver. $\pi/4$-shifted-DQPSK is essentially $\pi/4$-shifted-QPSK with differential encoding of the symbol phases. While the differential encoding protects against the loss of data due to channel phase slips, it also results in a loss of a pair of symbols when an error occurs. In a Rayleigh fading channel this translates to approximately a 3-dB loss in E_b/N_0 relative to coherent $\pi/4$-shifted-QPSK. $\pi/4$-shifted-DQPSK can be produced by either differentially encoding the source bits and mapping them onto absolute phase angles of a $\pi/4$-shifted-QPSK signal constellation or, alternately, by directly mapping the pairs of input bits onto the relative phases $(\pm\pi/4, \pm 3\pi/4)$. This second technique was used in the simulation described in this paper.

Differential detection or delay detection may be implemented at IF [4], [7] or at baseband [6], [7]. The baseband implementation allows a convenient realization on a digital signal processor (DSP). While the baseband implementations considered in [6] and [7] are based on sine-cosine detectors, the implementation discussed in this paper uses a tangent type differential detector with an integrated symbol timing and carrier frequency error estimation algorithm. This detector is less sensitive to carrier frequency errors and to amplitude variations in the received signal, relative to the sine-cosine detectors of [6] and [7].

It is widely accepted that the performance of differential detectors degrade rapidly in the presence of ISI. Consequently, a mobile unit employing a differential detector will not be able to meet the performance requirements for the U.S. digital cellular systems under multipath conditions [15]. In such cases an equalizer is required. However, when the ISI is small, the differential detection scheme considered here offers a simple and robust alternative to the more complex equalizer. Further, the detector presented here is easily modified to serve as a discriminator for analog FM demodulation. In this context our motivation is to study the performance of the tangent type differential detector in the mobile channel using U.S. digital cellular signaling specifications.

In this paper the BER performance of the tangent type differential detector is tested using the IS-54 specified TDMA frame structure [12] for base to mobile transmissions. Theoretical results, showing BER performance, are provided for static and Rayleigh fading channels. The sensitivity of the detector to Doppler, delay spread, symbol timing accuracy, and carrier frequency offsets is studied through simulations and corresponding results are reported. The simulations provide results for both E_b/N_0 and C/I.

Section II discusses the structure of the $\pi/4$-shifted-DQPSK transmitter that was used in the simulations. Section III presents the channel model and Section IV discusses the receiver structure. Section V derives the theoretical performance of the system and Section VI provides simulation results. Finally, Section VII presents some conclusions.

II. Transmitter

In the U.S., digital cellular system data is transmitted in a TDMA frame. A complete definition of the frame/slot structure for base-mobile and mobile-base transmission can be found in [1] and [12]. Fig. 2 illustrates the frame/slot structure used in the simulation.

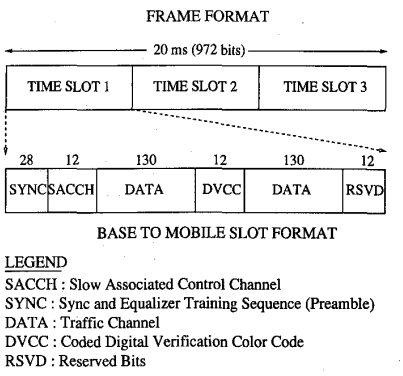

Fig. 2. IS-54 base mobile frame/slot structure.

TABLE I

b_{1k} (LSB)	b_{2k} (MSB)	$\delta\phi_k$
0	0	$\pi/4$
1	0	$3\pi/4$
1	1	$-3\pi/4$
0	1	$-\pi/4$

Fig. 3 is a block diagram of the transmission scheme used in the simulation study. Data to be transmitted is buffered and organized into the TDMA frame format as shown in Fig. 2. Next, bits b_{1k} and b_{2k} are paired (di-bits) and mapped onto differentially encoded signal phases, $\Delta\phi_k$, using a Gray code as illustrated in Table I. The $\pi/4$-shifted-DQPSK symbols, represented as a pair (I, Q), are then generated using the following relationship:

$$I_k = I_{k-1}\cos[\Delta\phi_k] - Q_{k-1}\sin[\Delta\phi_k] \tag{1}$$

$$Q_k = I_{k-1}\sin[\Delta\phi_k] + Q_{k-1}\cos[\Delta\phi_k] \tag{2}$$

where I_k and Q_k are the in-phase and quadrature components of the $\pi/4$-shifted-DQPSK signal corresponding to the kth symbol. Hence, if ϕ_k represents the absolute phase angle for the kth symbol, basic trigonometric identities can be used to express (1) and (2) as

$$I_k = \cos[\phi_k] = \cos[\phi_{k-1} + \Delta\phi_k] \tag{3}$$

$$Q_k = \sin[\phi_k] = \sin[\phi_{k-1} + \Delta\phi_k]. \tag{4}$$

The symbols are then pulse shaped using a square root raised cosine filter which has a frequency response of the form

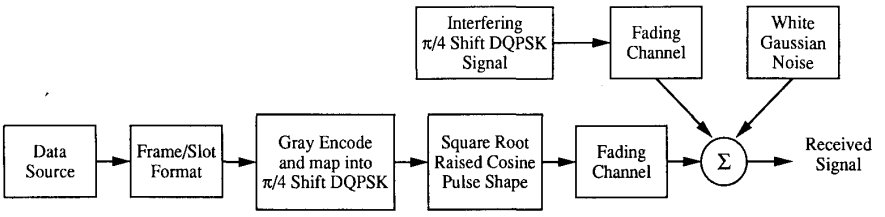

Fig. 3. Transmitter and channel used in simulation.

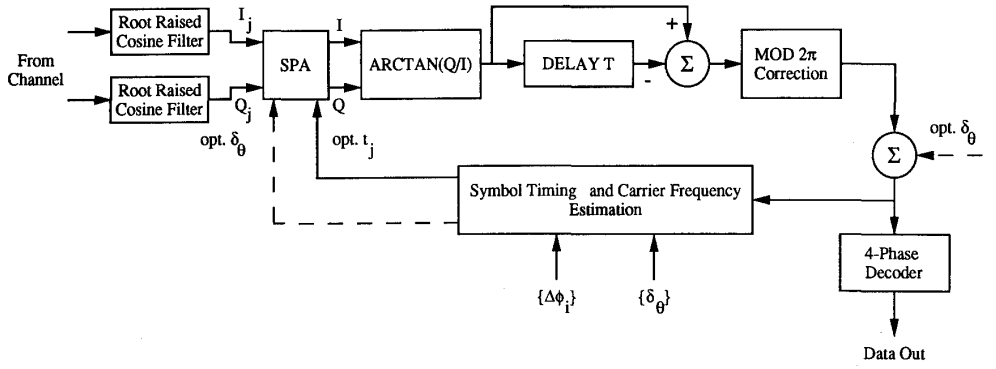

Fig. 4. Block diagram of the demodulator/detector.

$$|G(f)| = \begin{cases} T, & 0 \le |f| \le \frac{(1-\alpha)}{2T} \\ T\sqrt{\frac{1}{2}\left\{1-\sin\left[\pi\frac{T}{\alpha}\left(|f|-\frac{1}{2T}\right)\right]\right\}}, & \frac{(1-\alpha)}{2T} \le |f| \le \frac{(1+\alpha)}{2T} \\ 0, & |f| > \frac{(1+\alpha)}{2T} \end{cases} \tag{5}$$

where α is the roll-off factor and T is the symbol period. Alternately, the square root raised cosine filter can be expressed in terms of its impulse response which can be shown to be

$$g(t) = \begin{cases} 1-\alpha+4\frac{\alpha}{\pi}, & t=0 \\ \frac{\alpha}{\sqrt{2}}\left[\left(1+\frac{2}{\pi}\right)\sin\left(\frac{\pi}{4\alpha}\right)+\left(1-\frac{2}{\pi}\right)\cos\left(\frac{\pi}{4\alpha}\right)\right], & t=\pm\frac{T}{4\alpha} \\ \frac{\sin\left[\pi(1-\alpha)\frac{t}{T}\right]+4\alpha\frac{t}{T}\cos\left[\pi(1+\alpha)\frac{t}{T}\right]}{\pi\frac{t}{T}\left[1-\left(4\alpha\frac{t}{T}\right)^2\right]}, & \text{for all other } t \end{cases} \tag{6}$$

The derivation for this impulse response is provided in Appendix I.

In an actual transmitter, the pulse shaped signal is then modulated onto the carrier, amplified by a power amplifier and transmitted. If the power amplifier is assumed to be linear, the transmitted signal can be represented as

$$s(t) = \sum_n g(t-nT)\cos(\omega_c t + \phi_n) \tag{7}$$

where, ω_c is the angular carrier frequency.

In the simulation, the final step of placing the signal on a carrier is omitted and the baseband in-phase and quadrature signals are passed to the channel model. While the results in this paper do not consider the effect of nonlinearities in the power amplifier, nonlinear amplification, and its effect on ACI are considered in [16].

III. Channel

The baseband transmitter outputs are processed by the channel simulation and passed to the receiver. Simulation results are presented later in the paper for a static channel, a Rayleigh fading channel, and a discrete multipath channel. For E_b/N_0 measurements, white Gaussian noise is used as additive interference in each of the channels. For C/I measurements, a second $\pi/4$-shifted-DQPSK signal is used as additive interference. In this case, the relative symbol timing between the communication and interfering signals is varied uniformly over the interval $\pm T/2$ on a slot-by-slot basis. The discrete multipath channel is modeled as a two ray model with both rays Rayleigh faded with equal average power and shifted in frequency by a Doppler spread proportional to the vehicle speed, as described in [13]. The delay interval or delay spread, (τ) between the two rays is expressed in terms of symbol periods. The rms delay spread, for this two ray model, is one half the delay interval between the two rays.

IV. Receiver

Fig. 4 is a block diagram of the receiver. The receiver obtains two parallel streams of samples of the baseband $\pi/4$-shifted-DQPSK signal, I_j and Q_j, from the channel. In an actual receiver, these sample streams would be derived from a received RF signal, possibly using a digital complex sampling system such as those described in [6] and [8]. In the simulation the I_j and Q_j sample streams each contain eight samples per symbol.

These input sample streams are first filtered by square root raised cosine filters which are matched to those in the transmitter. The outputs from the filters are then processed by the symbol and phase adjust (SPA) block which selects one sample per symbol from each of the I_j and Q_j streams and applies a correction for the carrier frequency offset. By selecting one sample per symbol, the receiver is essentially performing symbol timing recovery. The choice of the best sample time is made by the symbol timing and carrier frequency estimator using an algorithm which is described in a later section. In addition, the symbol timing and carrier frequency estimator produces an estimate of the carrier offset between the received signal and the local oscillator. The SPA takes this estimate and applies a frequency correction by phase rotating the sampled signal by an amount proportional to the estimate of the frequency offset in a direction opposite to the original rotation.

The outputs from the SPA are sent to the differential detector which consists of an arctangent function to extract the signal phase and a difference function which determines the phase change over one symbol interval. Following the difference function, it is necessary to apply the modulo-2π correction logic which corrects for errors created by the angles wrapping around the real axis. If $\Delta\phi_k$ is the difference between ϕ_k and ϕ_{k-1}, which are the phase angles of the kth and k–1th symbols respectively, then mod-2π correction is applied as

$$\begin{aligned} &\text{IF} \quad \Delta\phi_k < -180^\circ \quad \text{THEN} \quad \Delta\phi_k = \Delta\phi_k + 360^\circ \\ &\text{IF} \quad \Delta\phi_k > 180^\circ \quad \text{THEN} \quad \Delta\phi_k = \Delta\phi_k - 360^\circ. \end{aligned} \tag{8}$$

The need for this correction is explained by the following example: Let $\phi_k = 10^\circ$, $\phi_{k-1} = 340^\circ$ Then, without the mod-2π correction, $\Delta\phi_k = -330^\circ$, when it should actually be $\Delta\phi_k = 30^\circ$. Thus the mod-2π correction removes the wrap-around error about the positive real axis.

The corrected relative phase angle is decoded directly into a pair of bits (di-bits) by using decoding logic that determines which quadrant the resulting angle is in. The decoding logic outputs the binary value (2 bits) corresponding to the quadrant number minus one. The quadrants are numbered in an anticlockwise direction, starting from the positive real axis, as 1-2-3-4. For a Gray coded transmitted bit stream the quadrants are numbered in an anticlockwise direction as 1-2-4-3.

The same basic detector structure can be used as a discriminator for demodulating analog FM or detecting $\pi/4$-shifted-DQPSK. In both these cases, samples are sent to the arctangent function at a higher rate and the differencing operation is performed with a shorter delay. For example, the differential detector discussed above can be modified so that all eight samples per symbol are sent to the arctangent function. The phase difference operation now has a shorter delay (one-eighth of a symbol period versus a full symbol period) because of the higher sampling rate. For analog FM demodulation, the output of the difference operation will be the demodulated signal and the symbol timing and carrier frequency offset estimation will be disabled. For detecting $\pi/4$-shifted-DQPSK, it is necessary to perform an integrate-and-dump operation prior to the phase decoder. The symbol timing and carrier frequency offset estimation would be the same as in the differential detection case except the symbol timing would control the integrate-and-dump rather than the SPA.

A. Symbol Timing and Frequency Offset Estimation

Symbol timing estimation involves choosing a sample point in each symbol interval which will minimize BER. Symbol timing errors result in the inclusion of inter-symbol interference components. Carrier frequency offset is the frequency error between the local oscillator at the receiver and the received carrier. The carrier frequency offset results in a constant phase rotation per symbol in a specific direction. One result of carrier frequency offset is that the baseband square root raised cosine filters are no longer matched to the input signal. This mismatch results in degradation of BER performance.

Two techniques that address symbol timing and frequency offset estimation are described in [9] and [10]. The scheme described here is similar in concept to those of [9] and [10], in the context of choosing symbol timing and frequency offset correction based on optimizing a metric expressed in terms of the two parameters. However, in each of these schemes a different metric has been chosen for obtaining an estimate of symbol timing and frequency error correction. The metrics used in the three schemes are described below.

The scheme of [9] estimates timing and phase correction based on minimizing the time averaged squared vector difference between the received signal samples and a known sequence. The minimization is performed over the amplitude, timing and phase of the known sequence via a three-dimensional search. The known sequence can be either a preamble or decision directed symbols. The scheme can be simplified to a one-dimensional search as described in [9].

The scheme of [10] estimates timing using the absolute value of the phase difference between the received signal and the corresponding estimated symbol. Frequency offset is estimated using the phase difference (not absolute value) between the received signal phase and the detected signal phase. Subsequently, frequency offset is tracked using two phase locked loops operating on estimates provided by forward and backward decoding over the data block. The tracking is needed due to coherent detection.

The scheme described herein is based on maximizing the signal to impairment ratio with respect to timing and frequency offset. It is shown in Appendix II that this can be accomplished by minimizing the squared phase error, between a known preamble and the corresponding detected signal, with respect to the timing and frequency offset of the received signal. The minimization is done after differential detection. This scheme is of lower complexity than those of [9] and [10].

In the TDMA case, it is necessary to synchronize to a TDMA frame/slot prior to establishing symbol timing. This synchronization can be performed by correlating the preamble sequence contained within each slot with a local copy of the preamble sequence. We will assume that this timing can be established to be within $\pm N_1 (< N_s)$ samples of the true location, where N_s represents the number of samples per

symbol. Now, the best symbol timing location must be selected from

$$t_n = t_{\text{fsync}} \pm \frac{nT}{N_s} \tag{9}$$

where T is a symbol period, $n = 1, 2, \ldots N_s$ and t_{fsync} is the sample location corresponding to frame/slot sync.

In order to establish symbol timing, as described by (9), and estimate carrier frequency offset we perform a two-dimensional search to find the symbol time and phase rotation (corresponding to the frequency offset) that will optimize the following metric

$$\min_{\{t_j, \delta_\theta\}} \sum_{i=2}^{N_p} (\Delta\phi_i + \delta_\theta - \Delta\phi_i^e(t_j))^2 \tag{10}$$

where

$t_j =$ sample instant in each symbol,
$\Delta\phi_i =$ differential phase angle of ith symbol of preamble relative to the (i–1)th symbol,
$\delta_\theta =$ phase rotation per symbol period corresponding a quantized estimate of the frequency offset,
$\Delta\phi_i^e(t_j) =$ differential phase angle of the ith symbol corresponding to the t_jth sample instant, prior to decoding,
$N_p =$ number of symbols in the preamble.

If the magnitude of the phase jitter due to AWGN or co-channel interference is less that $\pi/2$ radians and there is no ISI, then the metric given by (10) is a rough approximation to choosing the largest maximum likelihood (ML) estimate of the signal to impairment ratio for each symbol time and frequency offset averaged over the preamble. A formal derivation of the above argument is provided in Appendix II.

An interesting feature of this symbol timing selection scheme is that it allows the sampling clock to be free running, i.e., not exactly locked to the symbol rate. However, the sampling clock must be close enough to an integer multiple of the symbol rate to insure that the symbol timing derived over the preamble remains reasonably accurate over the slot. Further, since the carrier frequency offset varies very slowly in comparison to the frame rate, carrier frequency offset estimation does not have to be done in every time slot. Only symbol timing adjustment needs to be done in every time slot. The performance of this scheme can be expected to degrade for long data slots and fast fading since the optimization is done only over a preamble sequence and, accordingly, it does not track changes which occur during the slot. In this case the scheme would have to be modified to include some type of tracking capability.

V. Theoretical Performance

In this section we provide expressions for evaluating the BER of the differential detector in a static and Rayleigh fading channel, based on the method of analysis presented in [5]. For Gray encoded $\pi/4$-shifted-DQPSK with equally probable signals the BER, in a static and Rayleigh fading channel, can be expressed as (see Appendix III)

$$\text{BER} = \int_{-\pi}^{\pi} \int_{\psi_2+\Delta\phi+\pi/4}^{\psi_2+\Delta\phi+5\pi/4} P(\psi_1|\phi_1)P(\psi_2|\phi_2)\, d\psi_1 d\psi_2. \tag{11}$$

Similarly, the average symbol error rate (SER), can be expressed as

$$\text{SER} = \int_{-\pi}^{\pi} \int_{\psi_2+\Delta\phi+\pi/4}^{\psi_2+\Delta\phi+7\pi/4} P(\psi_1|\phi_1)P(\psi_2|\phi_2)\, d\psi_1 d\psi_2 \tag{12}$$

where ψ_i, $i = 1,2$ and ϕ_i, $i = 1,2$ are the received and true phase angles of two successive transmitted symbols, respectively. ϕ_1 and ϕ_2 can take any of the following angles, $\phi_i = m\pi/4, m = 1, 2 \ldots 8$ under the constraint that $\Delta\phi = \phi_1 - \phi_2$ is $\pi/4$. Note that, for equally probable signals we need only consider one of four differential phase angles, for the purpose of BER calculation. $P(\psi_i|\phi_i), i = 1, 2$ represents the probability density function (pdf) of the detected phase angle given the correct phase angle.

A. Static Channel

For a static channel the pdf of ψ_i given ϕ_i can be shown to be

$$P(\psi_i|\phi_i) = \frac{1}{2\pi} e^{-2\gamma} \left[1 + \sqrt{8\pi\gamma}\cos(\phi_i - \psi_i) e^{2\gamma\cos^2(\phi_i - \psi_i)} \cdot \left\{1 - \frac{1}{2}\text{erfc}\left[\sqrt{2\gamma}\cos(\phi_i - \psi_i)\right]\right\}\right] \tag{13}$$

where

$$\text{erfc[X]} = \frac{2}{\sqrt{\pi}} \int_X^\infty e^{-t^2} dt$$

and γ is the SNR expressed as E_b/N_0.

It is noted that (13) is nothing but the pdf of the phase jitter due to AWGN, which is given in [14]. It is further noted that expressions similar to (11) and (13) have been previously derived in the context of limiter-discriminator detection in [5], and hold for the differential detector.

B. Rayleigh Fading

Assuming that the amplitude variations follow a Rayleigh pdf and that the channel induced phase remains constant over two symbol durations it can be shown, as in Appendix IV, that

$$P(\psi_i|\phi_i) = \frac{1}{2\pi(1+2\overline{\gamma})} + \frac{2}{\pi\overline{\gamma}} \frac{\cos(\phi_i - \psi_i)}{a^3(\phi_i - \psi_i)} \cdot \left[\frac{\pi}{2} - \mu(\phi_i, \psi_i) - \frac{1}{2}\sin[2\mu(\phi_i, \psi_i)]\right] \tag{14}$$

where

$$\mu(\phi_i, \psi_i) = \tan^{-1}\left[\frac{-2\cos(\phi_i - \psi_i)}{a(\phi_i, \psi_i)}\right]$$

$$a(\phi_i, \psi_i) = \sqrt{4\sin^2(\phi_i - \psi_i) + \frac{2}{\overline{\gamma}}}$$

and $\overline{\gamma}$ denotes the average SNR or average E_b/N_0.

The expressions given by (11), (12), and (14) also hold for limiter-discriminator detection.

When we have co-channel interference instead of AWGN, the expressions (11), (12), and (14) provide a good approximation to the BER and SER, respectively, by replacing $\overline{\gamma}$ by $\overline{\gamma}R_b/B_w$; where R_b is the bit rate and B_w is the equivalent two-sided noise bandwidth of the receive filter. This is because under Rayleigh fading the complex envelope of an interference signal is a zero mean complex Gaussian random variable, similar to AWGN, when conditioned upon the interfering symbol. For *a priori* equally likely interfering symbols the variance of the interfering signal is all that is needed to compute C/I. The corresponding value of C/I is $\overline{\gamma}R_b/B_w$. Under these conditions the BER or SER can be computed by using (14) in (11) or (12), respectively with the appropriate substitution for $\overline{\gamma}$.

VI. Simulation Results

In the simulation study we have assumed the IS-54 signaling specification for base-mobile transmission. Each TDMA frame is 20 ms long, comprising three time slots with each user transmitting every third slot. Each user transmits data in a 6.67 ms slot at a data rate of 48.6 kbps. Each slot has a single preamble (sync word) comprising 14 symbols located at the start of the slot. The transmitted symbols were sampled at eight times the symbol rate. A square root raised cosine filter, with a roll-off factor of 0.35 and truncated to 10 symbols, was used as the transmit filter. The receive filter had a square root raised cosine response which is matched to the transmit filter.

The BER performance was determined using a Monte Carlo simulation procedure. Each simulation was conducted over 1000 frames of data and averaged over three independent runs.

The frame/slot synchronization jitter was simulated by using a uniform random number generator to jitter the frame/slot timing within ± 4 samples about its true location. This value for the timing jitter is based on the assumption that initial frame/slot synchronization is established using two samples per symbol, which provides an accuracy to within $\pm 1/2$ symbol or ± 4 samples. The jitter was added at the beginning of each slot and subsequently, symbol timing was established and data decoded.

Frequency offset was added by rotating the received data samples by an amount equal to the slope of the frequency change between two successive samples. Carrier frequency offset correction was performed by estimating the corresponding phase rotation, using (10), and adding the correction to the differentially detected angle.

Fig. 5 illustrates theoretical and simulation results of BER versus E_b/N_0 for a static and Rayleigh fading channel. It is observed that for E_b/N_0 larger than 10 dB, the BER in Rayleigh fading is approximately equal to $0.5(E_b/N_0)^{-1}$. Fig. 5 also shows symbol error rate (SER), which is observed to be roughly twice the BER, as is expected with Gray encoding.

Fig. 6 illustrates BER versus E_b/N_0, plotted as a function of vehicle speed, considering the effect of symbol timing. This

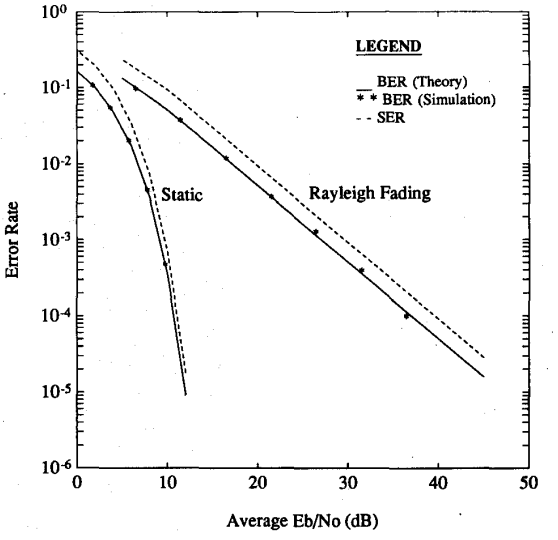

Fig. 5. BER versus E_b/N_0 for static and Rayleigh fading channels.

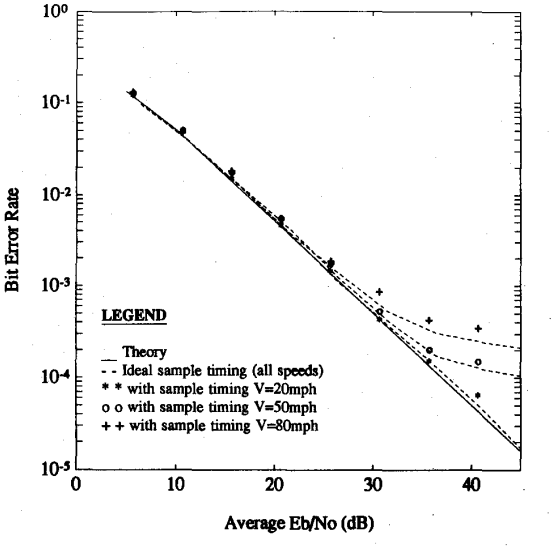
LEGEND
Theory
- - Ideal sample timing (all speeds)
* * with sample timing V=20mph
o o with sample timing V=50mph
+ + with sample timing V=80mph
Bit Error Rate
Average Eb/No (dB)

Fig. 6. BER versus E_b/N_0 as a function of vehicle speed in Rayleigh fading.

plot can also be interpreted in terms of the maximum Doppler frequency at 900 MHz. The maximum Doppler frequency is defined as $f_d(\max) = V/\lambda$; where V is the vehicle speed and λ is the carrier wavelength. The maximum Doppler frequencies corresponding to vehicle speeds of 20 mph, 50 mph, and 80 mph are 27 Hz, and 67 Hz, and 107 Hz, respectively. In the region above the irreducible error floor it is observed that the symbol timing algorithm of (10) results in a small E_b/N_0 loss (< 1 dB) relative to the case of ideal sampling. The degradation with higher vehicle speed is observed to be small.

Fig. 7 illustrates that the BER degrades rapidly with delay spread (τ), for the two ray channel described in Section III. A vehicle speed of 20 mph was assumed for this simulation.

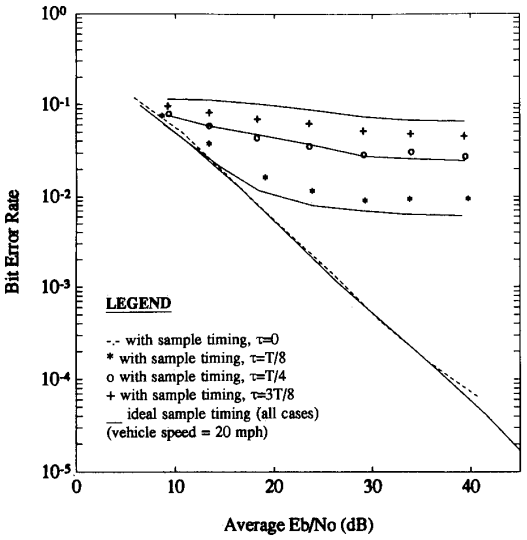
Bit Error Rate
Average Eb/No (dB)
LEGEND
-.- with sample timing, τ=0
* with sample timing, τ=T/8
o with sample timing, τ=T/4
+ with sample timing, τ=3T/8
__ ideal sample timing (all cases)
(vehicle speed = 20 mph)

Fig. 7. BER versus E_b/N_0 as a function of delay spread.

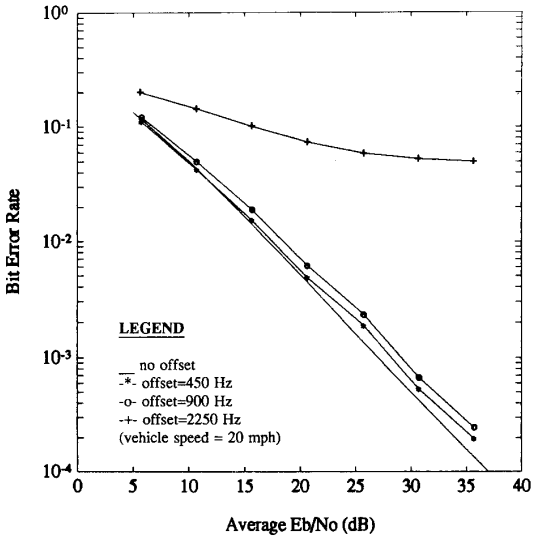

Fig. 8. BER versus E_b/N_0 as a function of carrier frequency offset without the offset correction.

From Fig. 7 it is seen that in order to obtain an uncoded BER of 3% at 17 dB E_b/N_0 the delay spread must be less than an eighth of the symbol period ($\approx 5\ \mu$s). It is interesting to note that the timing algorithm of (10) shows a slower rate of degradation than if timing were held at the ideal sampling instant corresponding to no delay spread.

Fig. 8 illustrates the BER degradation resulting from carrier frequency offset and Fig. 9 illustrates the corresponding BER when using the scheme of (10). A vehicle speed of 20 mph was assumed for these simulations. It is observed that there is negligible BER degradation for offsets less than approximately 450 Hz and frequency offset correction is not required, in the context of detection. For larger frequency offsets the correction scheme improves the BER. It is observed that when symbol timing is included with frequency offset correction there is some additional degradation over the case when ideal symbol timing is assumed due to errors associated with symbol timing estimation. However, for offsets less than 900 Hz no degradation was observed.

Figs. 10 through 12 provide performance results for co-channel interference. To obtain these results, a second $\pi/4$-shifted-DQPSK signal was used as an interferer. This interfering signal undergoes Rayleigh fading before being added to the faded communication (desired) signal. Fig. 10 gives BER performance as a function of C/I in Rayleigh fading. These curves are very similar to those of Fig. 6. Fig. 11 shows BER performance when the communication signal passes through a two-ray channel. As with AWGN performance degrades rapidly with delay spread. Finally, Fig. 12 shows the sensitivity of the receiver to frequency offsets. In general, the results for C/I and E_b/N_0 are quite similar.

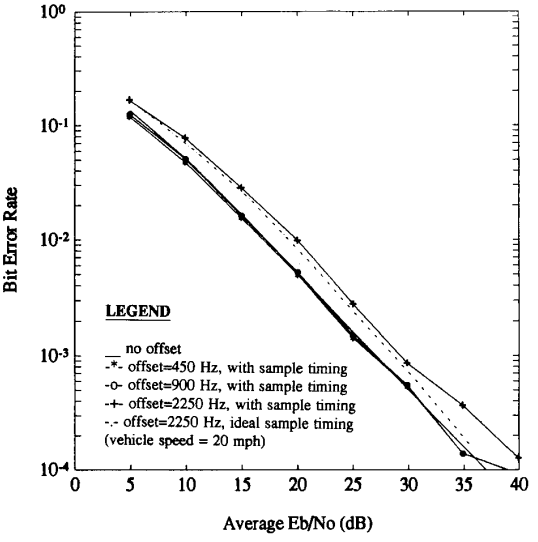
Bit Error Rate
Average Eb/No (dB)
LEGEND
__ no offset
-*- offset=450 Hz, with sample timing
-o- offset=900 Hz, with sample timing
-+- offset=2250 Hz, with sample timing
-.- offset=2250 Hz, ideal sample timing
(vehicle speed = 20 mph)

Fig. 9. BER versus E_b/N_0 as a function of carrier frequency offset with the offset correction.

VII. Conclusions

In this paper we have presented a tangent type differential detector with an integrated symbol timing and carrier frequency error estimation algorithm. The performance of this detector for $\pi/4$-shifted-DQPSK has been studied for base-mobile transmission using IS-54 signaling specifications. The BER in static and Rayleigh fading channels compares well with limiter-discriminator detection [3]–[5]. It is observed that the detector is sensitive to symbol timing errors and large carrier frequency offsets. For frequency offsets less than approximately 450 Hz there is negligible degradation, indicating that correction is not required. For the IS-54 base-mobile slot duration the timing algorithm offers acceptable performance in fast fading even with a short preamble of 14 symbols. The uncertainty associated with the proposed symbol timing and frequency offset estimation is due to the use of a sub-optimal metric and a short preamble and can be improved

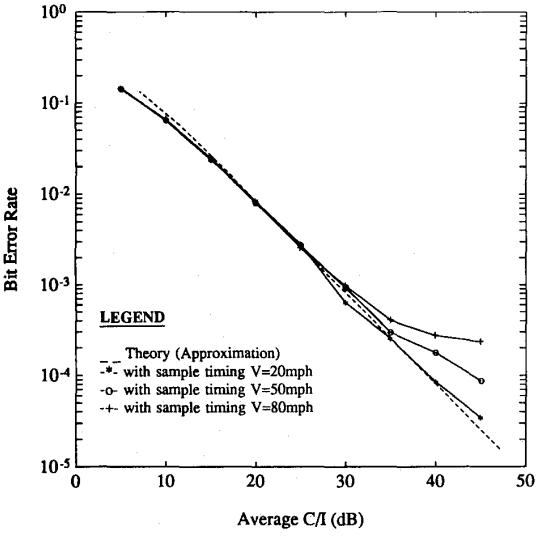

Fig. 10. BER versus C/I as a function vehicle speed in Rayleigh fading.

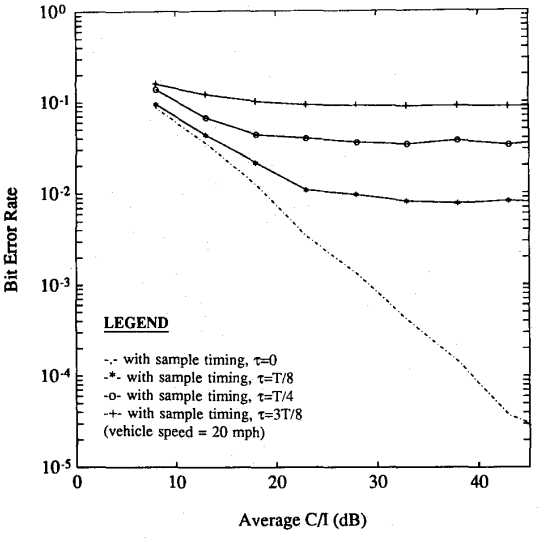
Bit Error Rate
Average C/I (dB)
LEGEND
-.- with sample timing, τ=0
-*- with sample timing, τ=T/8
-o- with sample timing, τ=T/4
-+- with sample timing, τ=3T/8
(vehicle speed = 20 mph)

Fig. 11. BER versus C/I as a function of delay spread.

by using a longer averaging period. Simulation results not presented herein indicate that the detector is insensitive to the roll-off factor of the transmit and receive filters. Further, the detector can be readily modified to demodulate an FM signal, a useful feature for a dual-mode receiver.

Although this detector is simple, robust and offers acceptable performance in a Rayleigh fading channel, its performance degrades very rapidly in a two-ray channel and hence does not meet the recommended minimum performance standards for U.S. digital cellular mobile receivers [15].

APPENDIX I
SQUARE ROOT RAISED COSINE IMPULSE RESPONSE

The transfer function of a square root raised cosine filter is given by

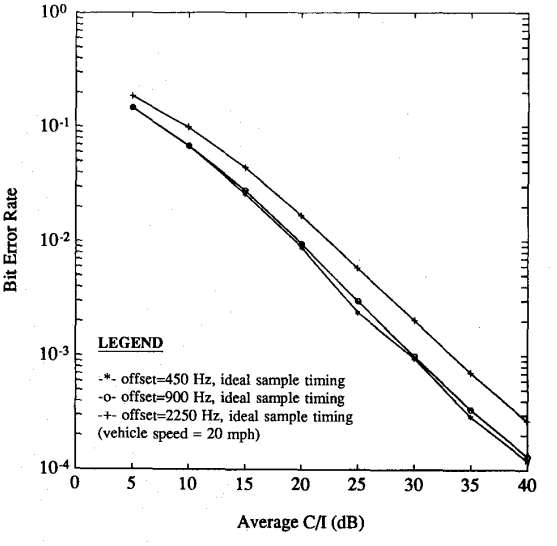
Bit Error Rate
Average C/I (dB)
LEGEND
-*- offset=450 Hz, ideal sample timing
-o- offset=900 Hz, ideal sample timing
-+- offset=2250 Hz, ideal sample timing
(vehicle speed = 20 mph)

Fig. 12. BER versus C/I as a function of carrier frequency offset with the offset correction.

$$G(f) = \begin{cases} T, & 0 \le |f| \le \frac{(1-\alpha)}{2T} \\ T\sqrt{\frac{1}{2}\left\{1-\sin\left[\pi\frac{T}{\alpha}\left(|f|-\frac{1}{2T}\right)\right]\right\}}, & \frac{(1-\alpha)}{2T} \le |f| \le \frac{(1+\alpha)}{2T} \\ 0, & |f| > \frac{(1+\alpha)}{2T}. \end{cases} \tag{A1.1}$$

The impulse response $g(t)$ is given by

$$g(t) = \int_{-\infty}^{\infty} G(f)e^{j2\pi ft}\,df. \tag{A1.2}$$

Since $G(f)$ is real and symmetric, then for real $g(t)$:

$$g(t) = 2\int_{0}^{\infty} G(f)\cos(2\pi ft)\,df. \tag{A1.3}$$

Using (A1.1) in (A1.3) we have

$$g(t) = 2T\int_{0}^{1-\alpha/2T} \cos(2\pi ft)\,df + 2\frac{T}{\sqrt{2}}\int_{1-\alpha/2T}^{1+\alpha/2T}\left[1-\sin\left(\frac{\pi T}{\alpha}\left(f-\frac{1}{2T}\right)\right)\right]^{1/2} \cdot \cos(2\pi ft)\,df. \tag{A1.4}$$

Defining $t' = t/T$ and solving the first integral we have

$$g(t) = \sin\left(\frac{\pi(1-\alpha)t'}{\pi t'}\right) + I_1 \tag{A1.5}$$

where

$$I_1 = \frac{2T}{\sqrt{2}} \int_{1-\alpha/2T}^{1+\alpha/2T} \left[1 - \sin\left(\frac{\pi T}{\alpha}\left(f - \frac{1}{2T}\right)\right)\right]^{1/2} \cos(2\pi f t)\, df. \tag{A1.6}$$

Using the substitution $f' = \frac{\pi T}{\alpha}\left(f - \frac{1}{2T}\right)$ in (A1.6) we have

$$I_1 = \frac{\alpha}{\pi\sqrt{2}} \int_{-\pi/2}^{\pi/2} 2\sqrt{1 - \sin(f')}\cos(2\alpha f' t' + \pi t')\, df'. \tag{A1.7}$$

Using the trigonometric identity $(1 - \sin(x)) = (\sin(x/2) - \cos(x/2))^2$ in (A1.7) and choosing the negative root so that the integral is positive, we have

$$I_1 = \frac{-\alpha}{\pi\sqrt{2}} \int_{-\pi/2}^{\pi/2} 2\left(\sin\left(\frac{f'}{2}\right) - \cos\left(\frac{f'}{2}\right)\right) \cdot \cos(2\alpha f' t' + \pi t')\, df'. \tag{A1.8}$$

Using the trigonometric identities $2\sin(A)\cos(B) = \sin(A+B) + \sin(A-B)$ and $2\cos(A)\cos(B) = \cos(A+B) + \cos(A-B)$ we have

$$\begin{aligned} I_1 = &-\frac{\alpha}{\pi\sqrt{2}} \int_{-\pi/2}^{\pi/2} \left[\sin\left(\left(\frac{1+4\alpha t'}{2}\right)f' + \pi t'\right) + \sin\left(\left(\frac{1-4\alpha t'}{2}\right)f' - \pi t'\right)\right] df' \\ &+ \frac{\alpha}{\pi\sqrt{2}} \int_{-\pi/2}^{\pi/2} \left[\cos\left(\left(\frac{1+4\alpha t'}{2}\right)f' + \pi t'\right) + \sin\left(\left(\frac{1-4\alpha t'}{2}\right)f' - \pi t'\right)\right] df'. \end{aligned} \tag{A1.9}$$

The integrations in (A1.9) are of the form

$$\int_a^b \sin(cx + d)\, dx = \frac{\cos(ca + d) - \cos(cb + d)}{c} \tag{A1.10a}$$

$$\int_a^b \cos(cx + d)\, dx = \frac{\sin(cb + d) - \sin(ca + d)}{c}. \tag{A1.10b}$$

Using (A1.10a) and (A1.10b) in (A1.9) and after some simple algebra we obtain

$$I_1 = \frac{4\alpha}{\pi} \frac{1}{1 - (4\alpha t')^2}\left[4\alpha t' \sin(\pi(1-\alpha)t') + \cos(\pi(1+\alpha)t')\right]. \tag{A1.11}$$

Using (A1.11) in (A1.5) combining terms and recalling that $t' = t/T$ yields

$$g(t) = \frac{\sin(\pi(1-\alpha)t/T) + 4\alpha t/T\cos(\pi(1+\alpha)t/T)}{\pi t/T\left[1 - (4\alpha t/T)^2\right]}. \tag{A1.12}$$

Note that $g(t)$ is not defined for $t = 0$ and $t = \pm T/4\alpha$. To evaluate $g(t)$ at these points we use L'Hôpital's rule on the function defined by (A1.12). The resulting impulse response is given by (6).

Appendix II
Metric for Timing and Frequency Offset Estimation

The sampled received baseband signal, corresponding to the kth symbol and sampling instant t_n, can be represented as

$$r_k(t_n) = g_k(t_n)e^{j(\phi_k + \theta_k(t_n))} + \nu_k(t_n) + \eta_k(t_n) \tag{A2.1}$$

where g_k is the amplitude of the signal, ϕ_k is the corresponding phase angle, θ_k is the channel induced phase shift, ν_k is the composite interfering signal and η_k is the AWGN component with zero mean and variance $2\sigma_n^2$. The noise and interference are assumed to be independent.

The interference ν_k is due to intersymbol interference (ISI), adjacent channel interference (ACI) and co-channel interference (CCI), and is assumed to be a zero mean complex Gaussian random variable with variance $2\sigma_v^2$. This is a practical approximation which simplifies the derivation of the metric.

For differential detection:

$$\begin{aligned} \Delta\psi_k(t_n) &= \psi_k(t_n) - \psi_{k-1}(t_n) \\ &= \tan^{-1}[r_k(t_n)r_{k-1}^*(t_n)]. \end{aligned} \tag{A2.2}$$

Using (A2.1) in (A2.2), expanding and neglecting the terms involving $[\nu_k(t_n)\nu_{k-1}^*(t_n)]$ and $[\eta_k(t_n)\eta_{k-1}^*(t_n)]$ (high SNR approximations) it can be shown that the conditional pdf of $\Delta\psi_k(t_n)$, in a quasi-stationary channel, is given by [14]

$$\begin{aligned} P(\Delta\psi_k(t_n) \,|\, \Delta\phi_k, \delta_\theta, \gamma_k(t_n)) = \\ \frac{1}{2\pi}e^{-\gamma_k(t_n)}[1 + \sqrt{4\pi\gamma_k(t_n)}\cos(\Delta\phi_k + \delta_\theta - \Delta\psi_k(t_n)) \\ e^{\gamma_k(t_n)\cos^2(\Delta\phi_k + \delta\theta - \Delta\psi_k(t_n))}(1 - \frac{1}{2}\mathrm{erfc}\left(\sqrt{\gamma_k(t_n)}\right) \\ \cos(\Delta\phi_k + \delta_\theta - \Delta\psi_k(t_n)))] \end{aligned} \tag{A2.3}$$

where $\Delta\phi_k = \phi_k - \phi_{k-1}$ and $\delta_\theta = \theta_k(t_n) - \theta_{k-1}(t_n)$ corresponds to the phase change over a symbol duration, due to frequency offset.

Further, the instantaneous signal-to-impairment ratio $\gamma_k(t_n)$ in (A2.3) is defined as

$$\gamma_k(t_n) = \frac{g_k^2(t_n)}{4(\sigma_\nu^2 + \sigma_N^2)}. \tag{A2.4}$$

For $\gamma_k(t_n) \gg 1$ and $|(\Delta\phi_k + \delta_\theta - \Delta\psi_k(t_n))| < \frac{\pi}{2}$, (A2.3) can be approximated as [14]

$$P(\Delta\psi_k(t_n) \mid \Delta\phi_k, \delta_\theta, \gamma_k) = \sqrt{\frac{\gamma_k(t_n)}{\pi}}\, e^{-\gamma_k(t_n)\sin^2(\Delta\phi_k+\delta_\theta-\Delta\psi_k(t_n))} \tag{A2.5}$$

The ML estimate of $\gamma_k(t_n)$ is a solution to

$$\frac{\partial}{\partial\gamma_k(t_n)} \ln \mathrm{P}(\Delta\psi_k(t_n) \mid \Delta\phi_k, \delta_\theta, \gamma_k(t_n)) = 0. \tag{A2.6}$$

Substituting (A2.5) in (A2.6) and solving yields

$$\hat{\gamma}_{\mathrm{ML}_k}(t_n) = \frac{1}{2\sin^2(\Delta\phi_k + \delta_\theta - \Delta\psi_k(t_n))}. \tag{A2.7}$$

Assuming the noise and interference are independent from sample to sample and that the channel is quasi-stationary over the preamble, we can use N_p samples to obtain a less noisy ML estimate as a solution to

$$\frac{\partial}{\partial\gamma(t_n)} \ln \prod_{k=1}^{N_p} P(\Delta\psi_k(t_n) \mid \Delta\phi_k, \delta_\theta, \gamma(t_n)) = 0. \tag{A2.8}$$

Solving (A2.8) using (A2.5) produces

$$\hat{\gamma}_{\mathrm{ML}}(t_n) = \frac{1}{\frac{1}{N_p}\sum_{k=1}^{N_p} 2\sin^2(\Delta\phi_k + \delta_\theta - \Delta\psi_k(t_n))}. \tag{A2.9}$$

The sample timing selection is based on maximizing the signal to impairment ratio over the preamble. Hence,

$$\max_{t_n} \gamma(t_n) = \min_{t_n} \sum_{k=1}^{N_p} 2\sin^2(\Delta\phi_k + \delta_\theta - \Delta\psi_k(t_n)). \tag{A2.10}$$

For $\gamma(t_n) \gg 1$, at the correct sampling point and for small deviations, $\sin(\Delta\phi_k + \delta_\theta - \Delta\psi_k(t_n)) \approx (\Delta\phi_k + \delta_\theta - \Delta\psi_k(t_n))$

Therefore, the sample timing estimation rule can be written as

$$\max_{t_n} \gamma(t_n) = \min_{t_n} \sum_{k=1}^{N_p} (\Delta\phi_k + \delta_\theta - \Delta\psi_k(t_n))^2. \tag{A2.11}$$

Equation (10) results from (A2.11) by setting $\Delta\psi_k(t_n) = \Delta\phi_k^e(t_n)$ and by reducing the summation by one term. It is to be noted that since δ_θ is not known *a priori* it is replaced by an estimate in (10) and the maximization is done over t_n and δ_θ.

APPENDIX III
BER ANALYSIS

From (A2.4) the phase angle of the sampled received signal is given by

$$\psi_k = \tan^{-1}\frac{g_k\sin(\phi_k+\beta_k)+\zeta_{qk}}{g_k\cos(\phi_k+\beta_k)+\zeta_{ik}}. \tag{A3.1}$$

We assume that the channel induced phase shift β_k remains constant over two symbol periods. Further, we assume that the phase shift is compensated as described in the paper. Hence, we set $\beta_k = 0$ in all future analysis.

The output of the differential detector is

$$\Delta\psi_k = \psi_k - \psi_{k-1}. \tag{A3.2}$$

The BER can be defined as shown in (A3.3), shown at the bottom of the page. For equally probable source symbols, assuming that $\Delta\phi_k = \phi_k - \phi_{k-1} = \pi/4$, the BER can be written as

$$\mathrm{BER} = \frac{P(\Delta\psi_k \varepsilon R_2) + P(\Delta\psi_k \varepsilon R_4) + 2P(\Delta\psi_k \varepsilon R_3)}{2} \tag{A3.4}$$

Similarly, the SER can be expressed as

$$\mathrm{SER} = P(\Delta\psi_k \varepsilon R_2) + P(\Delta\psi_k \varepsilon R_4) + 2P(\Delta\psi_k \varepsilon R_3). \tag{A3.5}$$

Due to symmetry, $P(\Delta\phi_k \varepsilon R_2) = P(\Delta\phi_k \varepsilon R_4)$. Hence,

$$\mathrm{BER} = P(\Delta\psi_k \varepsilon R_2) \tag{A3.6}$$

The decision regions may be expressed as

$$R_2: \Delta\phi_k + \frac{\pi}{4} \le \Delta\psi_k \le \Delta\phi_k + \frac{3\pi}{4} \tag{A3.7a}$$

$$R_3: \Delta\phi_k + \frac{3\pi}{4} \le \Delta\psi_k \le \Delta\phi_k + \frac{5\pi}{4} \tag{A3.7b}$$

$$R_4: \Delta\phi_k + \frac{5\pi}{4} \le \Delta\psi_k \le \Delta\phi_k + \frac{7\pi}{4} \tag{A3.7c}$$

Using (A3.2) we can rewrite (A3.7a), (A3.7b), (A3.7c) as

$$\psi_{k-1} + \Delta\phi_k + \frac{\pi}{4} \le \psi_k \le \psi_{k-1} + \Delta\phi_k + \frac{3\pi}{4} \tag{A3.8a}$$

$$\psi_{k-1} + \Delta\phi_k + \frac{3\pi}{4} \le \psi_k \le \psi_{k-1} + \Delta\phi_k + \frac{5\pi}{4} \tag{A3.8b}$$

$$\psi_{k-1} + \Delta\phi_k + \frac{5\pi}{4} \le \psi_k \le \psi_{k-1} + \Delta\phi_k + \frac{7\pi}{4}. \tag{A3.8c}$$

With (A3.8a), (A3.8b), and (A3.8c) defining the decision regions, the BER can be evaluated using the conditional joint pdf of ψ_k and ψ_{k-1}, which is given by

$$P(\psi_k, \psi_{k-1} \mid \phi_k, \phi_{k-1}) = P(\psi_k \mid \phi_k) P(\psi_{k-1} \mid \phi_{k-1}). \tag{A3.9}$$

$$\mathrm{BER} = \frac{(\text{no. of bit errors in decision region})(\text{prob. of phase lying in decision region})}{\text{number of bits per symbol}} \tag{A3.3}$$

The independence between ψ_k and ψ_{k-1} is due to the independence of the phase jitter due to the noise.

Now, using (A3.6), (A3.8a), (A3.8c), and (A3.9) the BER can be written as

$$\begin{aligned}\text{BER} = &\int_{-\pi}^{\pi}\int_{\psi_{k-1}+\Delta\phi_k+\pi/4}^{\psi_{k-1}+\Delta\phi_k+3\pi/4} P(\psi_k\,|\,\phi_k)P(\psi_{k-1}|\phi_{k-1})\,d\psi_k\,d\psi_{k-1}\\ &+\int_{-\pi}^{\pi}\int_{\psi_{k-1}+\Delta\phi_k+3\pi/4}^{\psi_{k-1}+\Delta\phi_k+5\pi/4} P(\psi_k\,|\,\phi_k)P(\psi_{k-1}|\phi_{k-1})\,d\psi_k\,d\psi_{k-1}\end{aligned} \tag{A3.10}$$

Equation (11) results from (A3.10) by combining the inner integrals.

Similarly, (12) can be obtained from (A3.5), (A3.8a), (A3.8b), (A3.8c), and (A3.9).

Appendix IV
PDF of Phase Jitter under Rayleigh Fading

The conditional pdf of the phase jitter $\psi_k - \phi_k$ is given by (13) and may be rewritten as

$$\begin{aligned}P(\psi_k\,|\,\phi_k,\gamma) = \frac{1}{2\pi}e^{-2\gamma}\Big[1+\sqrt{8\pi\gamma}\cos(\phi_k-\psi_k)\\ \cdot\, e^{2\gamma\cos^2(\phi_k-\psi_k)}\\ Q[-2\sqrt{\gamma}\cos(\phi_k-\psi_k)]\Big]\end{aligned} \tag{A4.1}$$

where

$$Q[X] = \frac{1}{\sqrt{2\pi}}\int_X^\infty e^{-t^2}\,dt\,.$$

The pdf of γ under Rayleigh fading is given by [14]

$$P(\gamma) = \frac{1}{\overline{\gamma}}e^{-\frac{\gamma}{\overline{\gamma}}}\;\gamma > 0 \tag{A4.2}$$

where $\overline{\gamma} = \boldsymbol{E}(\gamma)$ is the average value of E_b/N_0.

The conditional pdf of the phase jitter averaged over γ with respect to (A4.2) is

$$P(\psi_k\,|\,\phi_k) = \int_0^\infty P(\psi_k\,|\,\phi_k,\gamma)P(\gamma)\,d\gamma \tag{A4.3}$$

Using, (A4.1) and (A4.2) in (A4.3) we have

$$\begin{aligned}P(\psi_k|\phi_k) = &\frac{1}{2\pi\overline{\gamma}}\int_0^\infty e^{-(2+1/\overline{\gamma})}d\gamma\\ &+\frac{1}{\overline{\gamma}}\int_0^\infty\frac{\sqrt{\gamma}}{\pi}\cos(\phi_k-\psi_k)e^{-(2\sin^2(\phi_k-\psi_k)+1/\overline{\gamma})\gamma}\\ &\int_{-2\sqrt{\gamma}\cos(\phi_k-\psi_k)}^\infty e^{-t^2/2}\,dt\;d\gamma\,.\end{aligned} \tag{A4.4}$$

Making the substitution $x = \frac{t}{\sqrt{\gamma}}$, interchanging the order of integration in the second term in (A4.4) and simplifying we have

$$P(\psi_k|\phi_k) = \frac{1}{2\pi}\frac{1}{1+2\overline{\gamma}} + I_d \tag{A4.5}$$

where I_d is given by

$$\begin{aligned}I_d = &\frac{1}{\pi\overline{\gamma}}\int_{-2\cos(\phi_k-\psi_k)}^\infty\cos(\phi_k-\psi_k)\\ &\cdot\int_0^\infty\gamma e^{-\left(2\sin^2(\phi_k-\psi_k)+1/\overline{\gamma}+x^2/2\right)\gamma}d\gamma\;dx\,.\end{aligned} \tag{A4.6}$$

The inner integral is of the form

$$\int_0^\infty X^{N-1}e^{-AX}dX = \frac{\Gamma[N]}{A^N}. \tag{A4.7}$$

Using (A4.7) in (A4.6) and rewriting we have

$$I_d = \frac{1}{\pi\overline{\gamma}}\cos(\phi_k-\psi_k)\int_{-2\cos(\phi_k-\psi_k)}^\infty\frac{4}{\left(a^2(\phi_k,\psi_k)+x^2\right)^2}\,dx \tag{A4.8}$$

where $a^2(\phi_k,\psi_k) = 4\sin^2(\phi_k-\psi_k)+\frac{2}{\overline{\gamma}}$.

Using the substitution $x = a(\phi_k,\psi_k)\tan(\psi)$ in (A4.8) and simplifying we get

$$I_d = \frac{4}{\pi\overline{\gamma}}\frac{\cos(\phi_k-\psi_k)}{a^3(\phi_k,\psi_k)}\int_{\mu(\phi_k,\psi_k)}^{\pi/2}\cos^2\psi\,d\psi \tag{A4.9}$$

where $\mu(\phi_k,\psi_k) = \tan^{-1}\left[\frac{-2\cos(\phi_k-\psi_k)}{a(\phi_k,\psi_k)}\right]$.

Using the trigonometric identity $2\cos^2(\theta) = 1+\cos(2\theta)$, integrating and simplifying we get

$$\begin{aligned}I_d = &\frac{2}{\pi\overline{\gamma}}\frac{\cos(\phi_k-\psi_k)}{a^3(\phi_k,\psi_k)}\\ &\cdot\left[\frac{\pi}{2}-\mu(\phi_k,\psi_k)-\frac{1}{2}\sin(2\mu(\phi_k,\psi_k))\right].\end{aligned} \tag{A4.10}$$

Equation (14) results from using (A4.10) in (A4.5).

Acknowledgment

The authors would like to thank A. Hassan and L. Ozarow for the useful discussions and helpful suggestions.

References

[1] C.-E. W. Sundberg and N. Seshadri, "Digital cellular systems for North America," in *Proc. Global Telecommunications Conf.*, Dec. 1990, San Diego, CA, vol. 1, pp. 533–537.

[2] F. G. Jenks, P. D. Morgan, and C. S. Warren, "Use of four-level phase modulation for digital mobile radio," *IEEE Trans. Electromagn. Compat.*, vol. EMC-14, pp. 113–128, Nov. 1972.

[3] Y. Akaiwa and Y. Nagata, "Highly efficient digital mobile communications with a linear modulation method," *IEEE J. Select. Areas Commun.*, vol. SAC-5, pp. 890–895, June 1987.
[4] S. H. Goode, H. L. Kazecki, and D. W. Dennis, "A comparison of limiter-discriminator, delay, and coherent detection for $\pi/4$-QPSK," in *Proc. IEEE Veh. Technol. Conf.*, May 1990, Orlando, FL, pp. 687–694.
[5] S. Ono, N. Kondoh, and Y. Shimazaki, "Digital cellular system with linear modulation," in *Proc. IEEE Veh. Technol. Conf.*, May 1989, San Francisco, CA, vol. 1, pp. 44–49.
[6] G. J. Saulnier and W. Rafferty, "DSP-based non-coherent dual detector demodulator for land mobile radio channels," in *Proc. IEEE Int. Conf. Commun.*, 1986, pp. 1008–1012.
[7] C. -L. Liu and K. Feher, "Non-coherent detection of $\pi/4$-QPSK systems in a CCI-AWGN combined interference environment," in *Proc. IEEE Veh. Technol. Conf.*, May 1989, San Francisco, CA, pp. 83–94.
[8] G. J. Saulnier, C. M. Puckette, R. C. Gauss, R. J. Dunki-Jacobs, and T. E. Thiel, "A VLSI demodulator for digital RF network applications : Theory and results," *IEEE J. Select Areas Commun.*, vol. 8, pp. 1500–1511, Oct. 1990.
[9] G. Ascheid, M. Oerder, J. Stahl, and H. Meyer, "An all digital receiver architecture for bandwidth efficient transmission at high data rates," *IEEE Trans. Commun.*, vol. 37, pp. 804–813, Aug. 1989.
[10] N. R. Sollenberger and J. C-I. Chuang, "Low-overhead symbol timing and carrier recovery for TDMA portable radio systems," *IEEE Trans. Commun.*, vol. 38, pp. 1886–1892, Oct. 1990.
[11] S. Ariyavisitakul and T. P. Liu, "Characterizing the effects of nonlinear amplifiers on linear modulation for digital portable radio communications," *IEEE Trans. Technol.*, vol. 39, pp. 383–389, Nov. 1990.
[12] *Cellular System: Dual Mode Mobile Station-Base Station Compatibility Standard,* EIA/TIA, Project 2398, Electronics Industries Association, Engineering Department, Oct. 1990.
[13] W. C. Jakes, *Microwave Mobile Communications.* New York: Wiley, 1974.
[14] J. G. Proakis, *Digital Communications.* New York: McGraw Hill, 1989.
[15] *Cellular System: Recommended Minimum Performance Standards for 800 MHz Dual-Mode Mobile Stations (DRAFT),* TR45.3, Project 2216, Oct. 1990.
[16] S. M. Hladik, S. Chennakeshu, and G. J. Saulnier, "ON ACIPR of $\pi/4$-Shifted-DQPSK for U.S. digital land mobile radio systems," in *Proc. IEEE Pacific Rim Conf. Commun., Computers and Signal Processing,* May 9–10, 1991, pp. 530–533.

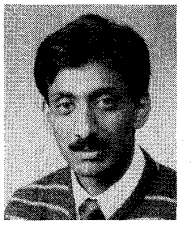

Sandeep Chennakeshu (S'85–M'88) received the B. Eng. degree in electronics from Bangalore University, India, in 1981, the Post Graduate Diploma in industrial management from the Indian Institute of Science, India in 1982, the M.Sc. degree in electrical engineering from the University of Saskatchewan, Canada, in 1984, and the Ph.D. degree in electrical engineering from Southern Methodist University, Dallas, TX, in 1988.

Since October of 1988 he has been with General Electric Co.'s Corporate R&D center in Schenectady, NY, working on mobile communication problems. His research interests are in cellular and land mobile radio, personal communication systems, and satellite communication.

Dr. Chennakeshu is the recipient of the Dennis Earle Memorial Award from the University of Saskatchewan and the Fredrick E. Terman Award from Southern Methodist Universtiy.

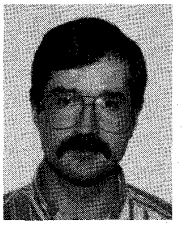

Gary J. Saulnier (S'80–M'84) was born in Fall River, MA on November 25, 1958. He received the B.S, M.E., and Ph.D. degrees in electrical engineering from Rensselaer Polytechnic Institute, Troy, NY, in 1980, 1982 and 1985, respectively.

In 1984, he joined General Electric Corporate Research and Development Center, Schenectady, NY, where he studied the design and implementation of bandwidth-efficient digital modulation techniques for fading channels. Since 1986, he has been on the faculty of the Electrical, Computer and Systems Engineering Department at Rensselaer Polytechnic Institute, where he is currently an Associate Professor. His research interests include modems for mobile and mobile-satellite channels, antijam spread spectrum communications systems, and electronic instrumentation.